Probing the growth quality of molecular beam epitaxy-grown Bi_2Se_3 films via in-situ Spectroscopic ellipsometry

Aofeng Bai[1], Maria Hilse[2], Prasanna D. Patil[5], Roman Engel-Herbert[2,3,4] †and Frank Peiris[1]*

*corresponding author e-mail: peirisf@kenyon.edu.edu

[1]Department of Physics, Kenyon College, Gambier, Ohio 43022, USA.

[2]Department of Materials Science and Engineering, Pennsylvania State University, State College, Pennsylvania 16802, USA.

[3]Department of Chemistry, Pennsylvania State University, State College, Pennsylvania 16802, USA.

[4]Department of Physics, Pennsylvania State University, State College, Pennsylvania 16802, USA.

[5]School of Physics and Applied Physics, Southern Illinois University Carbondale, Carbondale, Illinois 62901

†now at Paul-Drude-Institute for Solid State Electronics, Hausvogteiplatz 5-7, 10117 Berlin, Germany.

KEYWORDS

A3. Molecular Beam Epitaxy, A. Spectroscopic Ellipsometry, B. Topological Insulator, B. Bi_2Se_3, A. Dielectric Function, A. Thickness Control

ABSTRACT

Multilayer heterostructures of the topological insulator Bi_2Se_3 and conventional semiconductor In_2Se_3, as well as solid solution layers of $(Bi_{1-x}In_x)_2Se_3$ layers were grown by molecular beam epitaxy and analyzed in-operando using spectroscopic ellipsometry (SE). SE spectra were obtained after the deposition of each layer to determine the respective dielectric functions and thicknesses of each layer. In contrast to ex-situ SE, where uncertainty in the dielectric function and thicknesses of individual layer impose limitations to extract a correct model for the dielectric function of such multilayer heterostructures from a single set of SE data, the step-by-step in-situ SE data recover more precise dielectric functions for Bi_2Se_3, In_2Se_3, $(Bi_{0.7}In_{0.3})_2Se_3$ and the cap-layer. The optical models developed for multilayer structures can decipher minute perturbations in layers as the growth progresses. Our models show that a ~7 nm Bi_2Se_3 layer grown next to a sapphire substrate seems to disappear as the structure is annealed at 600 °C. Finally, when the dielectric functions were represented as a collection of Kramers-Kronig-consistent oscillators, in-situ SE predicted the quality of films; the weighted-average broadening parameter for oscillators used for Bi_2Se_3 films grown on $(Bi_{0.7}In_{0.3})_2Se_3$ layer is ~20% smaller compared to Bi_2Se_3 films directly grown on sapphire, confirming that the former film is of better quality, and providing a direct metric to quantify film quality and defect concentration. These conclusions were corroborated by transport data.

INTRODUCTION

Topological insulators (TIs) such as Bi_2Se_3 have attracted much attention in both fundamental and applied physics due in large to their unique optical, electrical and magnetic properties [1], [2]. Because of spin-orbit interaction and time reversal invariance, TIs form massless Dirac-like states with an intimate coupling between spin and momentum [3], [4], which can be exploited to realize novel functionalities predicted by theory, as well to produce interesting devices for applications in spintronics and quantum computing [5], [6]. The realization of TI-based devices requires high-quality thin film samples – grown by techniques such as molecular beam epitaxy (MBE) – that allow accessing the topological surface state (TSS) in TIs [7], [8].

Bi_2Se_3 films with sufficient quality to observe the topological non-trivial states have been realized before and can now be routinely obtained using MBE growth on a variety of substrates like Si, graphene, $SrTiO_3$ and sapphire [9], [10], [11], [12], [13], [14], [15], [16], [17] [7], [18], [19], [20], [21], [22]. The large number of unintentional carriers in the material caused by defects in the bulk or on interfaces dominate the transport properties over the TSS [23], [24], [25], [11], [21]. While compensation doping and anion or cation mixing are proven ways to reduce the number of free carriers, their incorporation into the lattice simultaneously cause a degradation of carrier mobilities [26], [27], [27]. To date, best results, i.e. lowest carrier densities with highest mobilities, have been realized by a buffer layer Bi_2Se_3 (BL-Bi_2Se_3) growth approach that suppresses both bulk and interfacial defect formation while preserving a high TSS mobility [28],[29]. Still substantial improvements in the synthesis are required to mature Bi_2Se_3 layers towards ‘electronic-grade’ material matching perfection of conventional semiconductor material.

Besides the availability of an array of ex-situ experimental tools to characterize the quality of MBE-grown Bi_2Se_3 films, it is imperative to use in-situ techniques, ideally operated in-operando during growth, to obtain immediate feed-back while the TI films are synthesized, so that the resulting films manifest the highest quality possible. Spectroscopic ellipsometry (SE) is a non-destructive optical method that can be employed to determine the dielectric function ($\varepsilon = \varepsilon_1 + i\varepsilon_2$) and the layer thickness of films in a structure [30]. Unlike alternative optical characterization techniques, such as transmission or reflectivity, SE does not require one to perform Kramers–Kronig transformation, and the dielectric function obtained from SE can be further analyzed to extract fundamental band gap as well as the higher order electronic transitions, therefore providing direct insights into the band structure of the material under study [31]. In analyzing SE spectra, experimental data must be fit to an optical model to obtain the dielectric function of the film. Such models can be unintentionally affected by the formation of over-layers and other contaminants, which can form when SE is performed ex-situ. While there are various methods to ameliorate issues related to modeling ex-situ SE spectra, such as representing the over-layers with appropriate dielectric functions and thicknesses, in general, both the precision and the accuracy of dielectric functions are compromised when SE is employed ex-situ [32]. The inherent shortcoming of SE as inverse-problem technique is particularly limiting when the sample of interest consists of several layers, where dielectric function and the thickness of each individual layer have to be determined by modeling a single set of SE data. For such samples, obtaining in-situ SE spectra —after the deposition of each layer— offer a more robust method to decipher the dielectric function of each layer with high precision and accuracy. In addition, the more reliable dielectric functions obtained via in-situ SE that are unobscured by surface reactions or adsorption layers can be further analyzed

to determine the quality of films [33] by using parametrization of the collection of oscillators specifying various electronic transitions as material quality metrics.

In this work, we investigated the dielectric properties of MBE-grown Bi_2Se_3, $(Bi_{0.7}In_{0.3})_2Se_3$ and In_2Se_3 films using *in-situ* SE. Using both single-layer films and multi-layer heterostructures, SE spectra were analyzed at each step of the growth cycle to obtain the dielectric function and the thickness of each layer. For the multilayer heterotructure, the detailed analysis shows that Bi_2Se_3 grown directly on sapphire substrate seems to disappear upon annealing the structure to 600 °C. The dielectric function found for each film via SE is modelled as a collection of oscillators, each of which is associated with an electronic transition in the material. This procedure allows us to infer the quality of films via the broadening parameter of oscillators. Specifically, we find that the Bi_2Se_3 films grown on a buffer layer of $(Bi_{0.7}In_{0.3})_2Se_3$ have a higher quality compared to Bi_2Se_3 grown directly on sapphire.

EXPERIMENTAL PROCEDURE

MBE growth was carried out on 10x10 mm^2 single crystal Al_2O_3 (0001) substrates purchased from Cryscore with a 0.2° miscut along the $[11\bar{2}0]$. Substrates were chemically cleaned using sequential ultrasonic baths of acetone, isopropyl alcohol, and DI water followed by a furnace anneal for 8 h at 1150 °C. After the furnace, substrates underwent a second chemical cleaning procedure identical to the initial routine but finished by a 40-min hot bath in nano-strip acid at 140 °C before thorough rinsing in DI water. Upon entering the ultra-high vacuum (UHV) system, a 30-min outgassing step at 120 °C was performed in the MBE system's load lock before transferring it to the model R450 MBE growth reactor (DCA Instruments) with a base pressure of 3×10^{-10} Torr. Se, Bi, and In were supplied by thermal evaporation from Knudsen effusion cells with typical

operation temperatures of around 140 °C, 535 °C, and 870 °C, respectively. Material fluxes were calibrated before growth using a quartz crystal microbalance (QCM) located at the substrate location with calibrated tooling factors determined from measuring the physical film thicknesses of Bi_2Se_3 and In_2Se_3 by X-ray reflectivity (XRR) and Se, and Si in scanning electron microscopy. Fluxes used for the grown of Bi_2Se_3 and In_2Se_3 layers were 1×10^{13} $cm^{-2}s^{-1}$ for the group-III and group-V constituents, and 1.3×10^{14} $cm^{-2}s^{-1}$, and 3×10^{13} $cm^{-2}s^{-1}$ for Se, and Si, respectively. For the growth of $(Bi_{0.7}In_{0.3})_2Se_3$, In and Bi fluxes were reduced to 2×10^{12} $cm^{-2}s^{-1}$, and 5×10^{12} $cm^{-2}s^{-1}$, respectively. Si was evaporated using an electron beam evaporator (Telemark) operated at a power of 400 W.

In-situ SE measurements were performed using a M-2000 in-situ ellipsometer model X-210 (J. A. Woollam). Spectra were recorded in the range from 210 nm to 1690 nm at a fixed angle setup of 75°. Routine calibration measurements of the SE were performed on a 25-nm-thick thermally grown native oxide layer on a Si wafer before each Bi_2Se_3 growth run to ensure that the SE data were not affected by unintentional alterations in the optical pathway, e.g. due to unintentional deposition of Se on optical viewports.

X-ray diffraction (XRD) was used to determine for structural evaluation in a Panalytical X'Pert3 4-circle diffractometer equipped with a PIXcel 3D detector. $CuK_{\alpha1}$ radiation was focused in high resolution configuration through a Ge(220) crystal hybrid attenuator with a 10 mm mask and a 1/32° slit onto the sample. For transport measurements, as grown films were scratched into Hall bar geometry (effective area ~ 1 mm × 0.5 mm) using computer-controlled probe station. Hall bars were contacted using Indium spheres to get an electric ohmic contact. Hall effect measurements were carried out using a Physical Property Measurement System (PPMS Quantum Design) with applied current of 1 μA.

SAMPLE GROWTH AND OVERVIEW

Four different types of samples were grown and analyzed. Sketches of the layer sequence, reflection high energy electron diffraction (RHEED) images taken along the $[11\bar{2}0]$ direction after the growth of the top most layer and before the deposition of the cap, *ex-situ* atomic force microscopy (AFM) images, and *ex-situ* out-of-plane XRD 2Θ-ω scans are presented in Fig. 1.

An initial 3-quintuple layer-thick (QL) Bi_2Se_3 film was deposited for all samples at 135 °C to obtain even surface coverage of the Al_2O_3(0001) substrate, followed by the growth of another 3 QL Bi_2Se_3 at 225 °C for samples A to C, and 27 QL Bi_2Se_3 at 225 °C for sample D ensuring a Se/Bi flux ratio larger than 10. The higher growth temperature increases the crystal quality of the Bi_2Se_3 film, demonstrated by the narrow high intensity streaks observed in RHEED, and the highly intense and narrow (0001)-oriented Bi_2Se_3 related diffraction peaks of 12^{th}, 15^{th}, and 18^{th} order in XRD for sample D.

Similarly, a 3-QL-thick In_2Se_3 layer was subsequently deposited onto the initial Bi_2Se_3 layer with a Se/Bi flux ratio larger than 10 at 225 °C for samples A to C, which was continued to a total thickness of 20 QL at a secondary growth temperature of 300 °C. The lower initial temperature for In_2Se_3 in the heterostructure was chosen to preserve the underlying Bi_2Se_3 template layer, which serves as nucleation template and ensures a high crystalline quality of the In_2Se_3 layer and showed an onset of desorption at 250 °C with a rate of about 1 QL every 10 min [34]. After this growth step, samples A to C were annealed in Se atmosphere to 600 °C for 10 min with a heating and cooling ramp rate of 20 K/min, to fully evaporate the buried Bi_2Se_3 nucleation template layer. This way, smooth and highly crystalline In_2Se_3 films – demonstrated by the streaky RHEED pattern and the presence of solely (0001)-oriented In_2Se_3 related diffraction peaks in XRD for sample B – were obtained on Al_2O_3. [28]

$(Bi_{0.7}In_{0.3})_2Se_3$ layers for samples A and C were grown with a Se/Bi flux ratio larger than 10 at 225 °C to limit Bi desorption from the film and ensure stoichiometry. Crystalline $(Bi_{0.7}In_{0.3})_2Se_3$ growth with smooth surfaces was achieved, resulting in high intensity RHEED lattice streaks for sample C and the double peak feature observed in XRD on the shoulder of the In_2Se_3 related diffraction peaks towards smaller 2Θ angles for all (0001)-oriented $(Bi_{0.7}In_{0.3})_2Se_3$ peaks of the 12th, 15th, and 18th diffraction order.

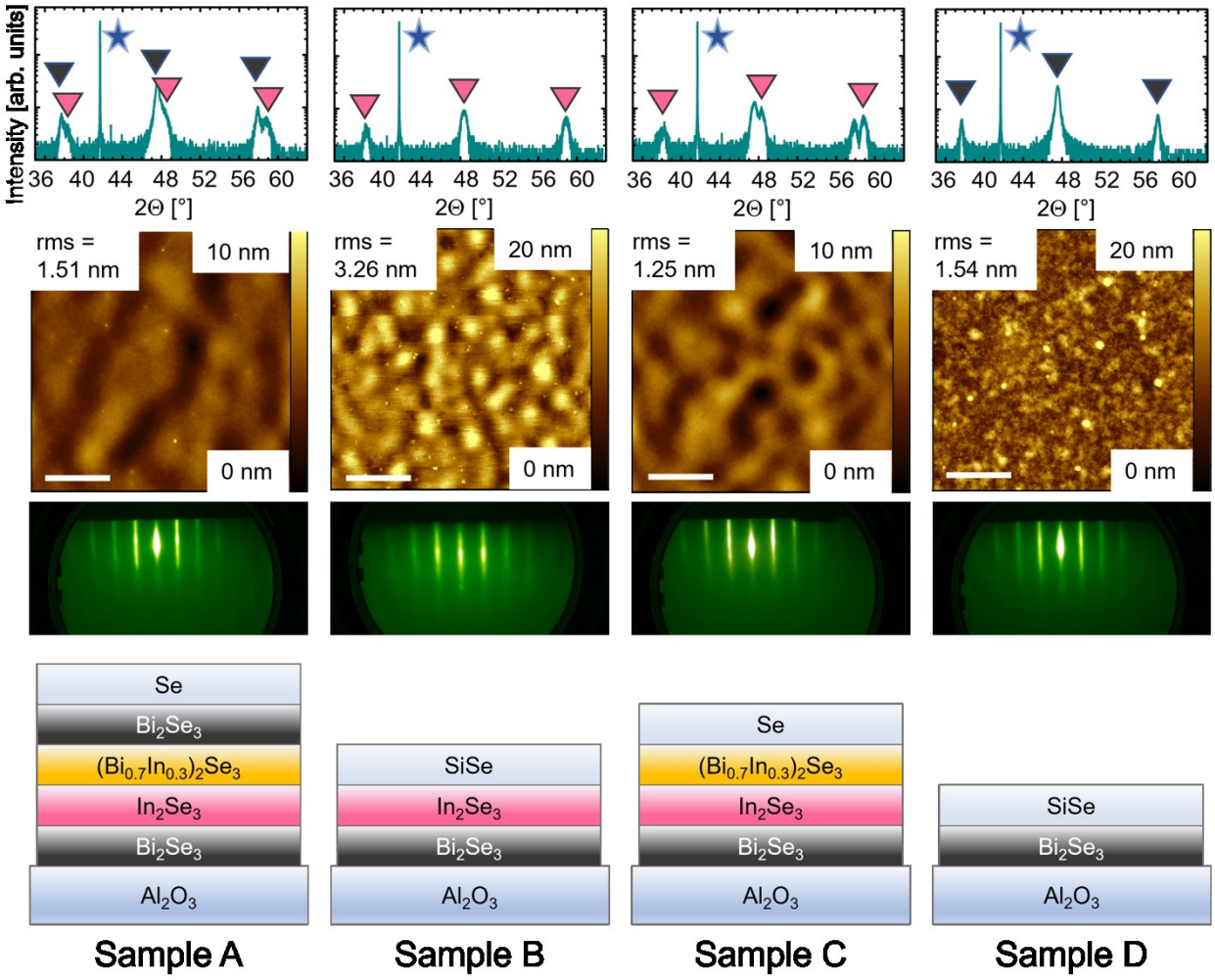

Figure 1. From bottom to top: sketch of the sample layer growth structures, RHEED images along the $[11\bar{2}0]$ direction observed after growth of the top most layer of each sample before the deposition of the capping layer, AFM images collected *ex-situ* on capped samples including the root-mean square (rms) roughness values (scale bar indicates 500 μm), out-of-plane XRD 2Θ-ω scans obtained *ex-situ* on capped samples (star: Al_2O_3 000 6 reflection, gray triangles: Bi_2Se_3 000 12 / 000 15 / 000 18 reflections, pink triangles: In_2Se_3 000 12 / 000 15 / 000 18 reflections). Note that for samples A and C, the $(Bi_{0.7}In_{0.3})_2Se_3$ layer also contributes to the diffraction peaks.

A final 20-QL-thick Bi_2Se_3 layer was grown at 225 °C on sample A with a flux ratio larger than 10, representing the BL-Bi_2Se_3 growth approach. Intense diffraction streaks in RHEED indicate a highly crystalline Bi_2Se_3 top layer with smooth surface. In the XRD scan, the Bi_2Se_3-related diffraction peaks dominate all other (In_2Se_3, and $(Bi_{0.7}In_{0.3})_2Se_3$-related) peaks in intensity and present as the narrowest, which is further prove of the high Bi_2Se_3 crystal quality.

All samples were capped with amorphous Se or SiSe layer that was deposited at room temperature in the MBE reactor to protect the chalcogenide films against moisture and oxidation in ambient pressure conditions, and enable *ex-situ* characterization. Even coverage of the samples by the capping material was monitored by RHEED. The intense diffraction patterns of all samples as shown in Fig. 1, disappeared completely, and turned into a dim diffuse background intensity typical for amorphous material after about 3 min into the capping layer growth, which was then continued for another 12 more min. Even coverage of the samples by the capping layer can also be deduced from the AFM images in Fig. 1, that reveal no particular terrace or thin film flake structure as these features are evenly buried under the cap layer.

Table 1. The layer structure and thickness values of the samples used for this study. The thickness values are obtained from SE models. For samples A, B & C, the original thickness of the first layer (Bi_2Se_3) changes to a much smaller value after the sample is annealed.

Sample	Layer 1 Thickness (nm)	Layer 2 Thickness (nm)	Layer 3 Thickness (nm)	Layer 4 Thickness (nm)	Layer 5 Thickness (nm)
A	Bi_2Se_3 7.1→0.19	In_2Se_3 9.9	$(Bi_{0.7}In_{0.3})_2Se_3$ 18.6	Bi_2Se_3 23.4	Se 27.1
B	Bi_2Se_3 7.2→0.22	In_2Se_3 9.6	SiSe 20.1		
C	Bi_2Se_3 7.1→0.25	In_2Se_3 9.8	$(Bi_{0.7}In_{0.3})_2Se_3$ 18.0	Se 26.6	
D	Bi_2Se_3 33.9	SiSe 20.6			

RESULTS

In general, SE measures the amplitude ratio Ψ and the phase shift Δ of orthogonally polarized light which are related to the ratio of reflection coefficients ρ by:

$$\rho = \frac{r_p}{r_s} = \tan(\Psi) \cdot e^{i\Delta}$$

with r_p and r_s the complex reflection coefficients for light polarized parallel and perpendicular to the plane of incidence, respectively [30]. Because the measured Ψ and Δ depend on the ε and the thickness of each layer of the structure, for ex-situ SE measurements, one has to model these properties of the entire structure for a given single set of Ψ and Δ values. Consequently, if the structure consists of several layers, this process becomes cumbersome, resulting in systematic uncertainties. One method to circumvent such uncertainties is to rely on in-situ spectra obtained after the deposition of each layer of the structure [32]. In the present study, since several layers

were grown on top of sapphire substrates, we are able to follow the growth cycle, layer-by-layer, to determine the ε and the thickness of each layer.

Figure 2 shows Ψ and Δ spectra obtained after the deposition of each layer for a representative sample (see sample A in Fig. 1 and Table 1). The individual layers that are sequentially deposited during the growth cycle are shown as insets in each panel of Fig. 2. Before depositing the first layer, Ψ and Δ spectra of only the sapphire substrate was obtained, as shown in the insert on Fig. 2a, and were fitted with available birefringent optical constants for sapphire [35], [36]. A good fit was obtained with values of zero for all three Euler angles, confirming that the optical axis of sapphire was the film plane normal [37], [38]. After obtaining the dielectric function of sapphire, we next move to analyze the first Bi_2Se_3 layer deposited on sapphire. As noted earlier, the first layer of Bi_2Se_3 consists of two sub-layers; an initial 3-QL layer deposited at 135 °C and another 3 QL layer deposited at 225 °C. Several methods to model these two sub-layers were tested. One model used different dielectric functions for the two Bi_2Se_3 sub-layers because they were deposited at two different temperatures. Another model incorporated rough layers between the sapphire and the first sub-layer of Bi_2Se_3, as well as between the two Bi_2Se_3 sub-layers. Comparing the goodness of fits for the different models, we found that best fits were obtained assuming a ~1-nm-thick rough layer between the sapphire and the first sub-layer of Bi_2Se_3. In this case the rough layer was modelled using an effective medium approximation [39]. Additionally, best fits were obtained when the two sub-layers of Bi_2Se_3 were merged into a single layer, assuming the same dielectric function (see Fig. 3a)

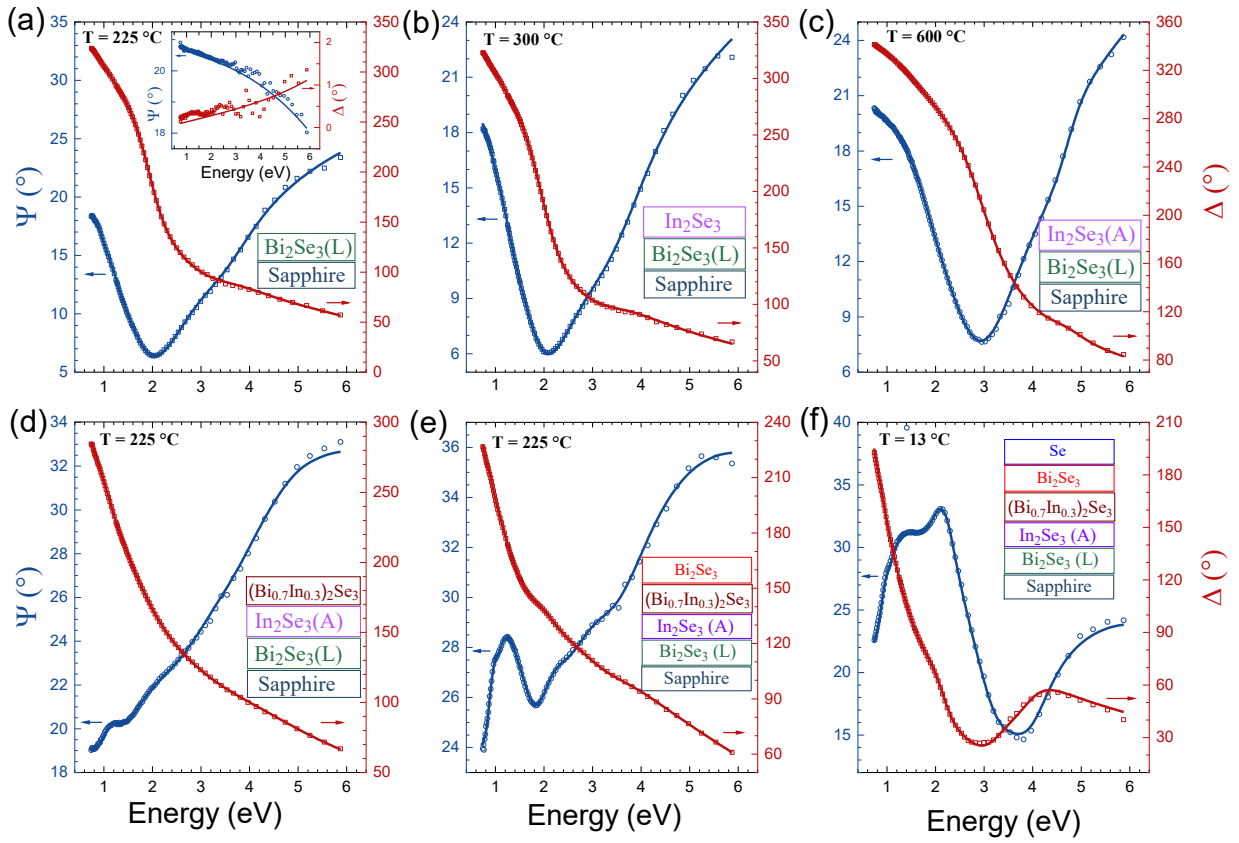

Figure 2. Data and fit of the parameters Ψ and Δ measured after the growth of each layer of a multilayer sample (see sample A Fig. 1 and Table 1). Starting from the sapphire substrate [shown in the insert in (a)], each panel shows the spectrum obtained after the deposition of the next layer (symbols) and the associated fit (solid lines) generated from the model, accounting for the thicknesses and the dielectric functions of the entire structure up to the top layer. Since this sample has two different Bi_2Se_3 films, the lower film is designated as Bi_2Se_3 (L). Since the In_2Se_3 layer changes after the annealing procedure, the changed layer is marked as In_2Se_3 (A).

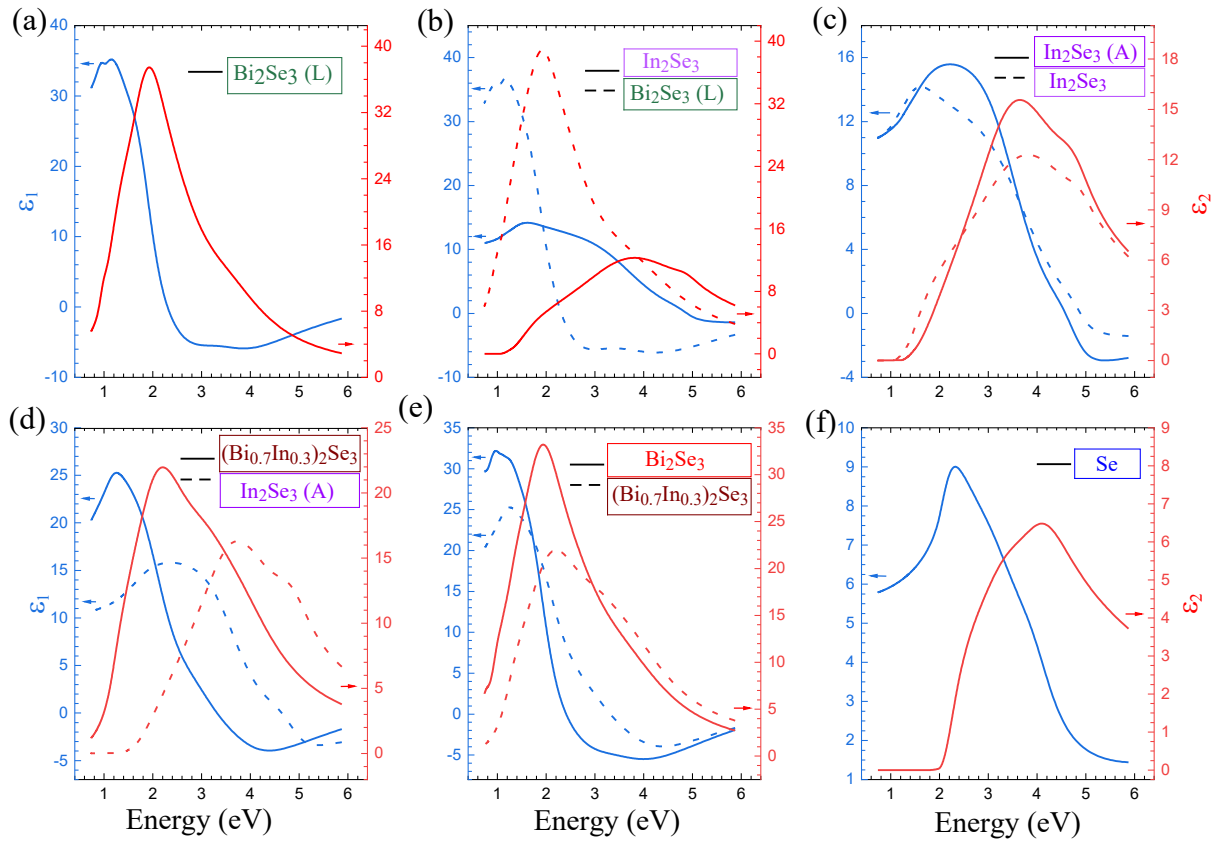

Figure 3. Real part ε_1 and imaginary part ε_2 of the dielectric function determined for the top layer corresponding to the growth of the multilayer structure depicted in Fig. (2). Panels b) through e) also shows the dielectric function of the multilayer structure on which the layer was grown by dashed lines.

In order to fit the experimental Ψ and Δ spectra (represented as symbols), the unknown parameters, both the ε and the thickness of Bi_2Se_3 were modelled to accomplish a suitable fit for the data. In this case, the ε of Bi_2Se_3 was represented with seven Kramers-Kronig consistent oscillators, whose amplitude, energy-position and broadening parameters were adjusted to obtain a fit, which is represented by a solid line in Fig. 2a [30]. In Fig. 3a, the corresponding ε of Bi_2Se_3 (both real and the imaginary parts) are shown. The dielectric function obtained for Bi_2Se_3 from this work was consistent with prior results [34],[40]. It is important to note that although Bi_2Se_3

will have an anisotropic dielectric function – due to its rhombohedral crystal structure – in this work we have assumed that its dielectric function is isotropic, as shown in Fig. 3a. Previous results have shown that if an anisotropic dielectric function is used for Bi_2Se_3, the effects on Ψ and Δ are barely noticeable [40].

After fitting Ψ and Δ spectra and obtaining the ε of Bi_2Se_3, we next move on to modeling the ε of the next layer of the structure, which is the In_2Se_3 layer deposited on the Bi_2Se_3 layer. Ψ and Δ spectra are shown in Fig. 2b for the combined three layers, consisting of the substrate, Bi_2Se_3 and In_2Se_3. Since the ε and the thickness of the bottom two layers are already known from the previous model that was generated to arrive at the fit depicted in Fig. 2a, only the In_2Se_3 top layer had to be modelled in order to recover a fit for Ψ and Δ spectra in 2b. Similar to the method used to fit the two sublayers of Bi_2Se_3, in this case too, we modelled the two In_2Se_3 layers (i.e., first 3-QL-thick layer deposited at 225 °C and the second 17-QL-thick layer deposited at 300 °C) as a single layer. Furthermore, an ~ 1nm rough layer was placed between Bi_2Se_3 and In_2Se_3. The solid lines in Fig 2b show the fit obtained in arriving at the ε of In_2Se_3 which was modelled with four oscillators. As shown in Fig. 3b, unlike in Bi_2Se_3 (indicated by the dashed lines) the ε_2 of In_2Se_3 is zero at lower energies, which signals the transparent range in this material. Hence, the first oscillator included to represent the ε of In_2Se_3 is associated with its fundamental energy gap, which we found to be 1.4 eV, a result that agrees with previous work [41]. While there are at least five polytypes of In_2Se_3, XRD results confirm that we attain the β polytype [42], [43]. The ε obtained for In_2Se_3 agrees with previously published results [44].

While the Ψ and Δ spectra in Figs. 2b and 2c are obtained for the same three-layer structure (i.e., sapphire, Bi_2Se_3 and In_2Se_3) of the sample, the difference in them indicates that the ε and the thicknesses of the three layers undergo changes as the sample is annealed in Se atmosphere at 600

°C for 10 min. As the spectra in Fig. 2c were taken at 600 °C, we let the ε of Bi_2Se_3 and In_2Se_3 change from the ones obtained at 300 °C (see Fig. 3b) while the ε for sapphire was assumed to be temperature independent due to its very large band gap [45]. The fitting procedure demanded that the original thickness of Bi_2Se_3 be reduced from 7.1 nm to 0.19 nm, signifying the near disappearance of the BL-Bi_2Se_3. Concurrently, the model also required a change in the ε of In_2Se_3 found at 300 °C, which is shown in Fig. 3c. Several alternative models were also developed and tested to fit the Ψ and Δ spectra obtained at 600 °C, including the incorporation of a $(Bi_{1-x}In_x)_2Se_3$ layer to accommodate the possibility of indium diffusion of into the Bi_2Se_3 layer [46], [47]. Such models did not yield the lowest chi-squared values and consequently, the best model obtained for the sample after the annealing procedure suggested that the Bi_2Se_3 layer was nearly removed along with a slight change in the ε of In_2Se_3 layer.

We followed the same procedure to obtain the ε of each subsequent layer and show the associated fits we obtained for Ψ and Δ (see Fig. 2d through Fig. 2f) along with the corresponding ε for each layer in Fig. 3d though 3f. In arriving at the fit for Ψ and Δ spectra in Fig. 2d, which was obtained at 225 °C, it was noticed that the ε of In_2Se_3 layer remained nearly the same as the annealed In_2Se_3 layer obtained at 600 °C. Previously we have found that the ε of Bi_2Se_3 remains fairly constant between 100 °C and 250 °C [34], as the ε of In_2Se_3 too did not change much with temperature. The optical model developed to fit the Ψ and Δ spectra in Fig. 2d also allowed to obtain the ε of the $(Bi_{0.7}In_{0.3})_2Se_3$ layer, which is shown in Fig. 3d. While this particular ternary alloy is not a TI [48], it is an important material that can be used as a growth template for other high-quality TIs, such as Bi_2Se_3. Hence the experimental determination of its ε is a prerequisite for producing TI-based devices. Compared to In_2Se_3 shown in Fig. 3d (dashed lines), both the real and the imaginary part of the dielectric function increased for $(Bi_{0.7}In_{0.3})_2Se_3$. In addition, the peak of

the ε_2 red-shifted in $(Bi_{0.7}In_{0.3})_2Se_3$, indicating a lowering of the band gap compared to In_2Se_3 [42]. To complete the entire growth cycle of sample A, we fit the Ψ and Δ spectra obtained in Fig 2e and 2f and obtain the dielectric functions for the Bi_2Se_3 layer grown on top of $(Bi_{0.7}In_{0.3})_2Se_3$, and the Se cap layer, which are shown in Fig. 3e and 3f. Figure 3e, which compared the dielectric functions of Bi_2Se_3 (solid lines) and $(Bi_{0.7}In_{0.3})_2Se_3$ (dashed-lines), indicates that in comparison to $(Bi_{0.7}In_{0.3})_2Se_3$, the peak of ε_2 red-shifted for Bi_2Se_3. In both Bi_2Se_3 and $(Bi_{0.7}In_{0.3})_2Se_3$, the peak of ε_2 was associated with a higher-order transition as their fundamental bandgap occurs at a lower energy than the spectral range covered by SE (i.e., 0.7 eV to 6 eV). This is indicated by the fact that ϵ_2 for both Bi_2Se_3 and $(Bi_{0.7}In_{0.3})_2Se_3$ is non-zero between 0.7 eV and 6 eV, unlike for In_2Se_3 (see Fig. 3c), where the transition from zero to non-zero in ε_2 occurred around 1.4 eV, signaling its fundamental bandgap. Finally, we note that the oscillator model developed to calculate the ε of Se places its optical bandgap at 2.05 eV, which agrees with previous results obtained for this amorphous semiconductor [49].

It is important to note that because the fits for Ψ and Δ spectra in Fig. 2 matched the experimental data, the associated ε obtained for each layer, as shown in Fig. 3, was reliable. Furthermore, since the ε and the thickness of each subsequent layer were modelled using the known parameters of the bottom layers, for any new set of Ψ and Δ only a few unknown parameters have to be incorporated into the new optical model. This is in contrast with ex-situ SE, where a single set of Ψ and Δ obtained after the growth of the entire structure – similar to the Ψ and Δ spectra in Fig 2f – has to be used to arrive at the ε and the thickness of each layer of the structure. In this case, one has to recover all of the unknown parameters by generating an optical model that fits a single set of Ψ and Δ, a task that compromises both accuracy and precision of the ε and the thickness of each layer.

As mentioned earlier, we found that the Bi_2Se_3 layer grown next to the sapphire substrate disappeared as the sample is annealed at 600 °C. In order to verify this phenomenon, we studied two more multilayer samples (Sample B and C in Table 1). Following the same procedure as described for Sample A, we obtained the dielectric functions and the thicknesses of each layer of the multilayer structure, before and after the annealing procedure. In Fig. 4, we show the thickness of each layer determined from modelling the SE spectra for all three samples. As in Sample A, our models confirm that the thickness of bottom Bi_2Se_3 layer reduces to about 0.2 nm (see Table 1) in both samples B and C as well. It is important to note that for all three samples, the value of the thickness found for the residual bottom Bi_2Se_3 layer from our models indicated an upper-bound value. Considering the uncertainty of thickness determined from our models (~0.2 nm), it is possible that the entire bottom Bi_2Se_3 layer disappeared due to the annealing procedure. In addition to confirming the near disappearance of the bottom Bi_2Se_3 layer, the analysis of samples B and C verified the dielectric functions of Bi_2Se_3, In_2Se_3, $(Bi_{0.7}In_{0.3})_2Se_3$ and the cap layer from analyzing Sample A.

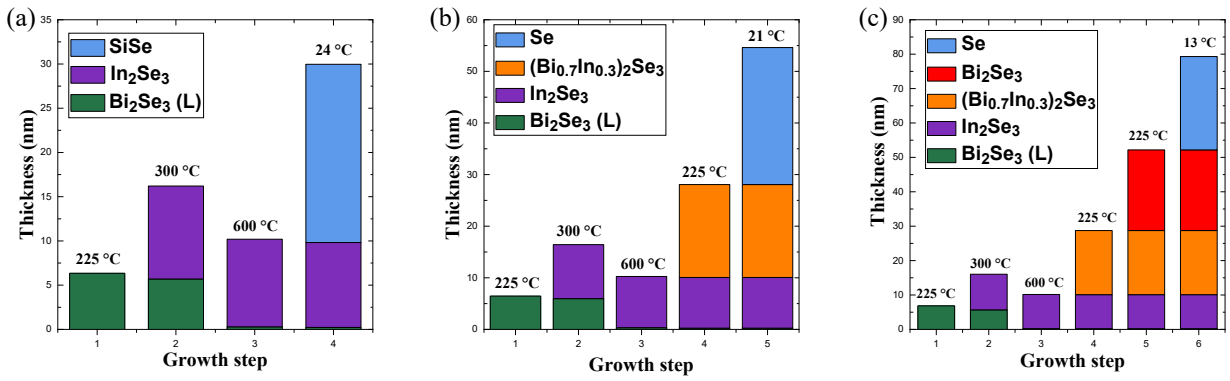

Figure 4. The thickness values of each layer determined by fitting specific Ψ and Δ spectra are shown for three samples; (a) sample B, (b) sample C and (c) sample A (see Table 1). Notice that

for all three samples, the bottom Bi_2Se_3 layer (indicated by green) disappeared after the annealing procedure.

As indicated before, the rationale for following a fairly complex MBE-growth procedure for sample A was to produce high-quality Bi_2Se_3. In this study, we were able to use SE to probe the difference between Bi_2Se_3 films grown on a $(Bi_{0.7}In_{0.3})_2Se_3$ layer (sample A in Table 1) and on a sapphire substrate (sample D in Table 1). In Fig. 5a, we show the dielectric functions of Bi_2Se_3 grown on these two layers, which have subtle variations. Compared to the Bi_2Se_3 film grown on the sapphire substrate, the imaginary part of ε for the Bi_2Se_3 grown on $(Bi_{0.7}In_{0.3})_2Se_3$ showed a reduction. In order to quantify the difference between the two dielectric functions carefully, the oscillator model making up the ε for these two layers was analyzed. The models and the parameters used for the ε for the two layers are shown in the supplementary materials. Out of the seven oscillators included to represent the ε Bi_2Se_3, only four pronounced oscillators are shown in Fig. 5b; the other three oscillators used to represent the ε have very small amplitudes (see table 1 in the supplementary materials; Fig. 5b shows the 4 oscillators labelled Lorentz 4 to Lorentz 6). While the oscillator centroids remained nearly constant for the two dielectric functions, the amplitude and the broadening parameters changed. To account for both of these changes, we have computed a weighted average for the broadening of all of the oscillators. This procedure allows us to consider the broadening of oscillators with higher amplitudes more than the ones with smaller amplitudes. These calculations showed that the broadening parameter for the Bi_2Se_3 grown on $(Bi_{0.7}In_{0.3})_2Se_3$ was around 20% smaller compared to that used for Bi_2Se_3 films grown on a sapphire substrate. Oscillator-broadening is commonly associated with the relaxation of momentum-conservation between electronic transitions due to a more pronounced electron scattering [33]. Conclusions

drawn from SE studies of these films were corroborated with transport measurements performed on the same films. Room-temperature Hall mobility was found to be 519 cm^2/Vs and 395 cm^2/Vs as well as charge carrier density of 1.1×10^{13} cm^{-2} and 5.7×10^{13} cm^{-2} for Bi_2Se_3 grown on $(Bi_{0.7}In_{0.3})_2Se_3$ and for Bi_2Se_3 grown directly on a sapphire, respectively. Having precise oscillator-models for the ε of Bi_2Se_3 allowed to directly evaluate the quality of films as they are grown in the MBE chamber, a clear advantage in growing high-quality TI films.

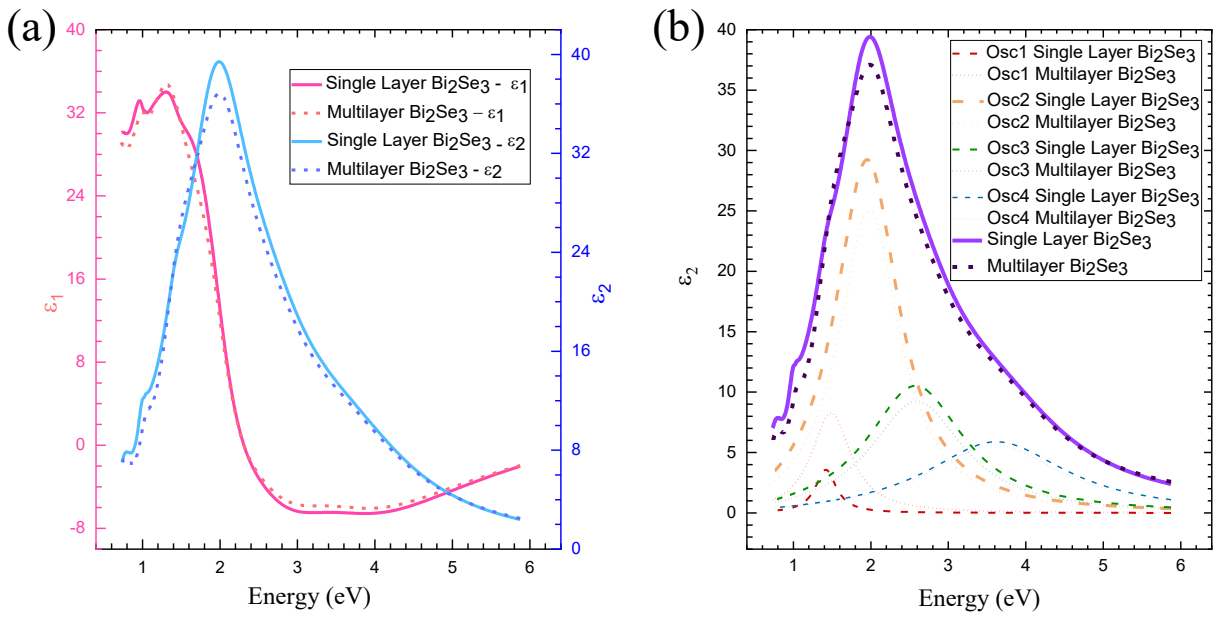

Figure 5. (a) Real (ε_1) and imaginary part (ε_2) of the dielectric function for Bi_2Se_3 grown on $(Bi_{0.7}In_{0.3})_2Se_3$ and on a sapphire substrate. (b) The four pronounced oscillators used to represent the ε of Bi_2Se_3 for both films.

CONCLUSIONS

The ε and thicknesses of individual layers were obtained by analyzing in-situ SE spectra taken after each growth step of a multilayer structure. In contrast to ex-situ SE, where one is privy to only a single set of Ψ and Δ spectra in order to determine a multitude of variables, in-situ SE allowed developing an optical model step-by-step, which greatly increased both accuracy and precision of the dielectric functions and thicknesses of individual layers. Evaluating the in-situ SE data of three multilayer films, we found that the upper limit of thickness of the Bi_2Se_3 layer grown next to the sapphire substrate is 0.2 nm, suggesting the near-disappearance of this layer after the annealing procedure. In order to explore how the quality of Bi_2Se_3 films depends on their growth procedure, we developed an oscillator model for ε, and found the weighted average of the broadening parameter of the oscillators that make-up the ε. Because the Bi_2Se_3 film grown on a $(Bi_{0.7}In_{0.3})_2Se_3$ layer has a lower weighted average of the broadening parameter, it has a superior quality in comparison to Bi_2Se_3 films grown on sapphire substrates.

AUTHOR INFORMATION

Corresponding Author

*e-mail: peirisf@kenyon.edu

DATA AVAILABILITY STATEMENT

All data that supports the findings of this study is available from the corresponding author upon reasonable request.

ACKNOWLEDGMENT

The work at Kenyon College was supported by the NSF grant DMR-2004812. This work at The Pennsylvania State University was facilitated by the Two-Dimensional Crystal Consortium – Materials Innovation Platform (2DCC-MIP) at The Pennsylvania State University, which is supported by NSF cooperative Agreement No. DMR-2039351. P.D.P. acknowledges the support provided by the Graduate School, Southern Illinois University Carbondale, through the Doctoral Fellowship and 2DCC-MIP, the Pennsylvania State University through Resident Scholar Visitor Program (RSVP).

References

[1] J. E. Moore, "The birth of topological insulators," *Nature*, vol. 464, no. 7286. pp. 194–198, Mar. 11, 2010. doi: 10.1038/nature08916.

[2] M. Z. Hasan and C. L. Kane, "*Colloquium* : Topological insulators," *Reviews of Modern Physics*, vol. 82, no. 4, Nov. 2010, doi: 10.1103/RevModPhys.82.3045.

[3] B. Yan and S. C. Zhang, "Topological materials," *Reports on Progress in Physics*, vol. 75, no. 9, 2012, doi: 10.1088/0034-4885/75/9/096501.

[4] M. Z. Hasan and J. E. Moore, "Three-Dimensional Topological Insulators," *Annual Review of Condensed Matter Physics*, vol. 2, no. 1, pp. 55–78, Mar. 2011, doi: 10.1146/annurev-conmatphys-062910-140432.

[5] X. L. Qi, T. L. Hughes, and S. C. Zhang, "Topological field theory of time-reversal invariant insulators," *Physical Review B - Condensed Matter and Materials Physics*, vol. 78, no. 19, Nov. 2008, doi: 10.1103/PhysRevB.78.195424.

[6] X. Zhang, J. Wang, and S.-C. Zhang, "Topological insulators for high-performance terahertz to infrared applications," *Physical Review B*, vol. 82, no. 24, Dec. 2010, doi: 10.1103/PhysRevB.82.245107.

[7] A. Richardella *et al.*, "Coherent heteroepitaxy of Bi2 Se3 on GaAs (111)B," *Applied Physics Letters*, vol. 97, no. 26, Dec. 2010, doi: 10.1063/1.3532845.

[8] G. Zhang *et al.*, "Quintuple-layer epitaxy of thin films of topological insulator Bi 2 Se3," *Applied Physics Letters*, vol. 95, no. 5, 2009, doi: 10.1063/1.3200237.

[9] Y. Ando, "Topological insulator materials," *Journal of the Physical Society of Japan*, vol. 82, no. 10. Oct. 2013. doi: 10.7566/JPSJ.82.102001.

[10] M. Vyshnepolsky, C. Klein, F. Klasing, A. Hanisch-Blicharski, and M. Horn-Von Hoegen, "Epitaxial growth of the topological insulator Bi2Se3 on Si(111): Growth mode, lattice parameter, and strain state," *Applied Physics Letters*, vol. 103, no. 11, Sep. 2013, doi: 10.1063/1.4821181.

[11] Y. S. Kim *et al.*, "Thickness-dependent bulk properties and weak antilocalization effect in topological insulator Bi2Se3," *Physical Review B - Condensed Matter and Materials Physics*, vol. 84, no. 7, Aug. 2011, doi: 10.1103/PhysRevB.84.073109.

[12] N. Bansal *et al.*, “Epitaxial growth of topological insulator Bi2Se3 film on Si(111) with atomically sharp interface,” *Thin Solid Films*, vol. 520, no. 1, pp. 224–229, Oct. 2011, doi: 10.1016/j.tsf.2011.07.033.
[13] X. Guo *et al.*, “Single domain Bi2Se3 films grown on InP(111)A by molecular-beam epitaxy,” *Applied Physics Letters*, vol. 102, no. 15, Apr. 2013, doi: 10.1063/1.4802797.
[14] M. Jamali *et al.*, “Giant Spin Pumping and Inverse Spin Hall Effect in the Presence of Surface and Bulk Spin-Orbit Coupling of Topological Insulator Bi2Se3,” *Nano Letters*, vol. 15, no. 10, pp. 7126–7132, Oct. 2015, doi: 10.1021/acs.nanolett.5b03274.
[15] A. Richardella, A. Kandala, J. S. Lee, and N. Samarth, “Characterizing the structure of topological insulator thin films,” *APL Materials*, vol. 3, no. 8, Aug. 2015, doi: 10.1063/1.4926455.
[16] B. Li, X. Guo, W. Ho, and M. Xie, “Strain in epitaxial Bi2Se3 grown on GaN and graphene substrates: A reflection high-energy electron diffraction study,” *Applied Physics Letters*, vol. 107, no. 8, Aug. 2015, doi: 10.1063/1.4929697.
[17] C. L. Song *et al.*, “Topological insulator Bi2 Se3 thin films grown on double-layer graphene by molecular beam epitaxy,” *Applied Physics Letters*, vol. 97, no. 14, Oct. 2010, doi: 10.1063/1.3494595.
[18] E. Falsetti *et al.*, “Infrared Spectroscopy of the Topological Surface States of Bi2Se3 by Use of the Berreman Effect,” *Physical Review Letters*, vol. 121, no. 17, Oct. 2018, doi: 10.1103/PhysRevLett.121.176803.
[19] N. Bansal, Y. S. Kim, M. Brahlek, E. Edrey, and S. Oh, “Thickness-independent transport channels in topological insulator Bi 2Se 3 thin films,” *Physical Review Letters*, vol. 109, no. 11, Sep. 2012, doi: 10.1103/PhysRevLett.109.116804.
[20] J. Hellerstedt, M. T. Edmonds, J. H. Chen, W. G. Cullen, C. X. Zheng, and M. S. Fuhrer, “Thickness and growth-condition dependence of in-situ mobility and carrier density of epitaxial thin-film Bi2Se3,” *Applied Physics Letters*, vol. 105, no. 17, Oct. 2014, doi: 10.1063/1.4900749.
[21] Y. H. Liu *et al.*, “Gate-tunable coherent transport in Se-capped Bi2Se3 grown on amorphous SiO2/Si,” *Applied Physics Letters*, vol. 107, no. 1, Jul. 2015, doi: 10.1063/1.4926624.
[22] J. Y. Park *et al.*, “Molecular beam epitaxial growth and electronic transport properties of high quality topological insulator Bi2Se3 thin films on hexagonal boron nitride,” *2D Materials*, vol. 3, no. 3, Sep. 2016, doi: 10.1088/2053-1583/3/3/035029.
[23] M. Brahlek *et al.*, “Disorder-driven topological phase transition in Bi 2 Se 3 films,” *Physical Review B*, vol. 94, no. 16, Oct. 2016, doi: 10.1103/PhysRevB.94.165104.
[24] M. Brahlek, N. Koirala, N. Bansal, and S. Oh, “Transport properties of topological insulators: Band bending, bulk metal-to-insulator transition, and weak anti-localization,” *Solid State Communications*, vol. 215–216, no. 1, pp. 54–62, 2015, doi: 10.1016/j.ssc.2014.10.021.
[25] D. Kim *et al.*, “Surface conduction of topological Dirac electrons in bulk insulating Bi 2 Se 3,” *Nature Physics*, vol. 8, no. 6, pp. 459–463, 2012, doi: 10.1038/nphys2286.
[26] Z. Ren, A. A. Taskin, S. Sasaki, K. Segawa, and Y. Ando, “Fermi level tuning and a large activation gap achieved in the topological insulator Bi 2Te 2Se by Sn doping,” *Physical Review B - Condensed Matter and Materials Physics*, vol. 85, no. 15, Apr. 2012, doi: 10.1103/PhysRevB.85.155301.

[27] J. G. Analytis, R. D. McDonald, S. C. Riggs, J. H. Chu, G. S. Boebinger, and I. R. Fisher, "Two-dimensional surface state in the quantum limit of a topological insulator," *Nature Physics*, vol. 6, no. 12, pp. 960–964, 2010, doi: 10.1038/nphys1861.
[28] N. Koirala *et al.*, "Record Surface State Mobility and Quantum Hall Effect in Topological Insulator Thin Films via Interface Engineering," *Nano Letters*, vol. 15, no. 12, pp. 8245–8249, Dec. 2015, doi: 10.1021/acs.nanolett.5b03770.
[29] N. Koirala, M. Salehi, J. Moon, and S. Oh, "Gate-tunable quantum Hall effects in defect-suppressed B i2 S e3 films," *Physical Review B*, vol. 100, no. 8, Aug. 2019, doi: 10.1103/PhysRevB.100.085404.
[30] H. Fujiwara, *Spectroscopic Ellipsometry*. Chichester, UK: John Wiley & Sons, 2007.
[31] M. Cardona, *Modulation Spectroscopy*. New York: Academic, 1969.
[32] J. N. Hilfiker, "In situ spectroscopic ellipsometry (SE) for characterization of thin film growth," in *In Situ Characterization of Thin Film Growth*, Elsevier Ltd, 2011, pp. 99–151. doi: 10.1533/9780857094957.2.99.
[33] H. v. Nguyen and R. W. Collins, "Finite-size effects on the optical functions of silicon microcrystallites: A real-time spectroscopic ellipsometry study," *Physical Review B*, vol. 47, no. 4, Jan. 1993, doi: 10.1103/PhysRevB.47.1911.
[34] M. Hilse, X. Wang, P. Killea, F. Peiris, and R. Engel-Herbert, "Spectroscopic ellipsometry as an in-situ monitoring tool for Bi2Se3 films grown by molecular beam epitaxy," *Journal of Crystal Growth*, vol. 566–567, p. 126177, Jul. 2021, doi: 10.1016/j.jcrysgro.2021.126177.
[35] I. H. Malitson, "Refraction and Dispersion of Synthetic Sapphire," *Journal of the Optical Society of America*, vol. 52, no. 12, Dec. 1962, doi: 10.1364/JOSA.52.001377.
[36] H. Yao and C. H. Yan, "Anisotropic optical responses of sapphire (α-Al2O3) single crystals," *Journal of Applied Physics*, vol. 85, no. 9, May 1999, doi: 10.1063/1.370184.
[37] D. Schmidt, "Characterization of highly anisotropic three-dimensionally nanostructured surfaces," *Thin Solid Films*, vol. 571, Nov. 2014, doi: 10.1016/j.tsf.2013.10.119.
[38] D. E. Aspnes, "Approximate solution of ellipsometric equations for optically biaxial crystals," *Journal of the Optical Society of America*, vol. 70, no. 10, Oct. 1980, doi: 10.1364/JOSA.70.001275.
[39] D. E. Aspnes, J. B. Theeten, and F. Hottier, "Investigation of effective-medium models of microscopic surface roughness by spectroscopic ellipsometry," *Physical Review B*, vol. 20, no. 8, Oct. 1979, doi: 10.1103/PhysRevB.20.3292.
[40] M. Eddrief, F. Vidal, and B. Gallas, "Optical properties of Bi $_2$ Se $_3$: from bulk to ultrathin films," *Journal of Physics D: Applied Physics*, vol. 49, no. 50, Dec. 2016, doi: 10.1088/0022-3727/49/50/505304.
[41] Y. Watanabe, S. Kaneko, H. Kawazoe, and M. Yamane, "Imperfections in amorphous chalcogenides. IV. A model of electrical conduction processes in amorphous and crystalline InSe," *Physical Review B*, vol. 40, no. 5, Aug. 1989, doi: 10.1103/PhysRevB.40.3133.
[42] J. Ye, S. Soeda, Y. Nakamura, and O. Nittono, "Crystal Structures and Phase Transformation in In2Se3 Compound Semiconductor," *Japanese Journal of Applied Physics*, vol. 37, no. 8, pp. 4264–4271, 1998.
[43] N. Balakrishnan *et al.*, "Quantum confinement and photoresponsivity of -In 2 Se 3 nanosheets grown by physical vapour transport," *2D Materials*, vol. 3, no. 2, p. 25030, Jun. 2016, doi: 10.1088/2053-1583/3/2/025030.

[44] Y. Wang and S. Law, "Optical properties of (Bi $_{1-x}$ In $_{x}$) $_{2}$ Se $_{3}$ thin films," *Optical Materials Express*, vol. 8, no. 9, Sep. 2018, doi: 10.1364/OME.8.002570.
[45] J. Y. Yang, W. J. Zhang, and L. H. Liu, "Anisotropic dielectric functions of (0001) sapphire from spectroscopic ellipsometry and first-principles study," *Physica B: Condensed Matter*, vol. 473, Sep. 2015, doi: 10.1016/j.physb.2015.05.032.
[46] H. D. Lee *et al.*, "Indium and bismuth interdiffusion and its influence on the mobility in In2Se3/Bi2Se3," *Thin Solid Films*, vol. 556, Apr. 2014, doi: 10.1016/j.tsf.2014.01.082.
[47] Y. Wang, T. P. Ginley, and S. Law, "Growth of high-quality Bi $_{2}$ Se $_{3}$ topological insulators using (Bi $_{1-x}$ In $_{x}$) $_{2}$ Se $_{3}$ buffer layers," *Journal of Vacuum Science & Technology B, Nanotechnology and Microelectronics: Materials, Processing, Measurement, and Phenomena*, vol. 36, no. 2, Mar. 2018, doi: 10.1116/1.5015968.
[48] M. Brahlek *et al.*, "Topological-Metal to Band-Insulator Transition in BiInSe Thin Films," *Physical Review Letters*, vol. 109, no. 18, Oct. 2012, doi: 10.1103/PhysRevLett.109.186403.
[49] L. B. Schein, "Charge generation from band-gap states in amorphous selenium films," *Physical Review B*, vol. 10, no. 8, Oct. 1974, doi: 10.1103/PhysRevB.10.3451.